JOURNAL OF GEOPHYSICAL RESEARCH, VOL. 105, NO. B10, PAGES 23,879–23,894, OCTOBER 10, 2000

Evidence for temporal variation of seismic velocity within the upper continental crust

Götz H. R. Bokelmann[1]
Department of Geophysics, Stanford University, Stanford, California

Hans-Peter Harjes
Institut für Geophysik, Universität Bochum, Bochum, Germany

Abstract. Observations of systematic temporal variations of seismic anisotropy are presented for an induced-seismicity experiment at 9 km depth. These observations were made under particularly well-controlled conditions in the German Continental Deep Drilling Program (KTB) borehole, using shear wave splitting from similar events recorded at a three-component instrument located at 4 km depth from a hydraulic fracturing experiment at 9 km depth. In a large set of seismic events recorded during the experiment, many can be associated with multiplets exhibiting essentially identical waveforms. Since they must have approximately the same source location and source radiation pattern, these events are particularly useful for testing the hypothesis of time-dependent anisotropy. Anisotropy itself is clearly a very prominent feature in the data. A simple approach for waveform matching of split shear waves allows unprecedented resolution of variations in shear wave splitting. Importantly, the variation of shear wave splitting with time is a relative measurement, which can be performed with higher accuracy than the associated absolute measurement. In particular, the relative measurement is not affected by timing errors nor by event distance variations. During the experiment the difference between shear wave velocities decreases by $\sim 2\%$ within ~ 12 hours. After that, the medium apparently approaches a state which is stable for at least 5 hours. We suggest that the temporal variation is due to the tectonic stress release from seismic events caused by the fluid injection. This model requires the presence of fluid-filled cracks at depths larger than 4 km.

1. Introduction

There is little doubt that anisotropy is an important feature of elastic wave propagation throughout many regions of the Earth: It affects apparent velocities of P waves [e.g., *Hess*, 1964], polarization of P waves [e.g., *Bokelmann*, 1995a], and particularly shear waves [e.g., *Ando et al.*, 1983]. Such effective anisotropy at seismic wavelengths of 10^{-1} to 10^{2} km can be caused by a variety of effects, all of which are associated with some type of ordering in the medium. These effects range from preferential orientation of minerals (each with its own intrinsic anisotropy), layering, to preferentially oriented cracks or faults. These effects may have about the same order of magnitude and often similar angle dependence, which makes a distinction usually rather difficult, unless some of the effects can be ruled out on other grounds. Generally, however, all of these effects are present, and the question is only to which degree they contribute to the observations. An important question is whether or not effective anisotropy changes with time. Such temporal variations (at least those on timescales of years or less), if they can be found, narrow down the choice to just few effects. More importantly, however, temporal variations would show that (and perhaps how) anisotropy reacts sensitively to changes in the stress field and it might perhaps serve as a simple means for measuring crustal stress changes at reasonable cost [*Crampin and Zatsepin*, 1997].

Several observations have been suggested, which appear to show a time dependence of anisotropy. These observations are in all cases associated with variations in shear wave splitting. *Gupta* [1973] presented apparent observations of very large temporal variations, which were soon disputed on grounds that they might also be explained by scattering and phase conversions

[1]Previously at Institut für Geophysik, Ruhr-Universität Bochum, Germany.

Paper number 2000JB900207.
0148-0227/00/2000JB900207$09.00

within the crust [*Ryall and Savage*, 1974]. *Peacock et al.* [1988] and *Crampin et al.* [1990] present observations of shear wave splitting from local events near the Anza Gap in California, where one station apparently shows very large variations of shear wave splitting over just weeks before and after a nearby event. These splitting delay time data, however, were disputed by *Aster et al.* [1990], who used a different approach of estimating shear wave splitting: while *Peacock et al.* [1988] and *Crampin et al.* [1990] extracted the time separation between the two shear wave phases (splitting delay) by visually inspecting waveforms, Aster et al. (1990) estimated the splitting delay as the length of the time interval of linearly polarized shear wave motion. Most of the data both groups used were from indiscriminate regional seismicity. We believe, however, that the argument can be sharpened considerably by special techniques for similar events (doublets), which are nearly colocated and similar in source radiation pattern. In contrast, regional seismicity contains events of strongly varying character. However, depending on the focal mechanisms, which may differ between events, relative amplitudes of fast and slow shear wave phases may differ substantially. This may affect either method. An ideal approach would either use identical events or at least take the focal mechanism differences into account explicitly. In our study, similar events are found by a cluster analysis procedure: Since events are often remarkably similar in source location and focal mechanism, a waveform matching technique allows determination of variations in shear wave splitting with unprecedented resolution. Using several clusters of events, we show that the delay between split shear waves indeed varies with time. Distance variation of the events within a cluster are estimated with similar resolution. Anisotropy, as recorded by the shear wave splitting varies by $\sim$ 2.5% over just a few hours.

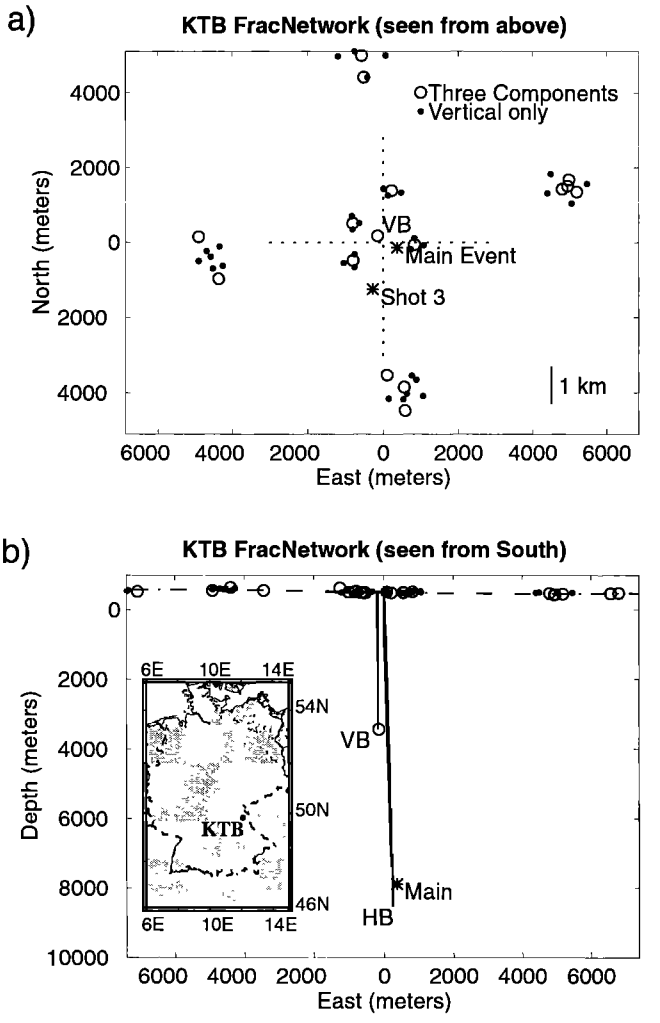

Figure 1. The "Kontinentale Tiefbohrung" KTB in the Oberpfalz region of southeastern Germany; instrument deployment during the Frac Experiment 1994 shown (a) top and (b) side view. Three-component receivers are shown by open circles, single (vertical) component instruments by dots. Note the location of the borehole instrument "Vorbohrung" VB in Figure 1b), which supplied the data in this paper, and the bottom of the KTB drillhole ("Hauptbohrung" HB), where fluid was injected during the experiment. The location of one particularly large event ("main event") and a surface shot (shot 3) are also shown.

2. Experiment

The "Kontinentale Tiefbohrung" (German Continental Deep Drilling Program) KTB is a scientific deep drilling project in the Oberpfalz region of southeastern Germany (Figure 1). Since 1990, drilling has progressed to the final depth of 9101 m below the surface. One of the last experiments performed at that depth was the KTB Frac Experiment 1994, which is discussed in detail by *Zoback and Harjes* [1997]. The goals of that experiment were related to studying the behavior of the crust at that deep level in the crust during hydrofracturing; in particular, one goal was to determine the stress field acting at that depth, which has never before been obtained by direct observation. Pumping started at 2202:15 UTC on December 17, 1994, and lasted for about a day. During and after the experiment, flow rate, pressure, and seismicity were closely recorded (Figure 2). The experiment was conducted in two phases: first the frac-phase lasting for $\sim$ 9 hours and second the main fluid injection phase lasting until $\sim$ 23 hours after the start. A large number of seismic events were generated during each of these phases. There were 376 events with magnitudes of at least -2.1, the *b* value is 1.1. More details of the event location distribution and focal mechanisms are given in *Zoback and Harjes* [1997].

2.1. Main Event and Anisotropy

During the 2-day interval a magnitude 1.2 event occurred, which was more than a magnitude larger than the second largest event. That event, which we refer to as the "main event", a recorded with excellent signal-to-noise ratio on all stations temporarily installed for the experiment and also on stations of the German Regional

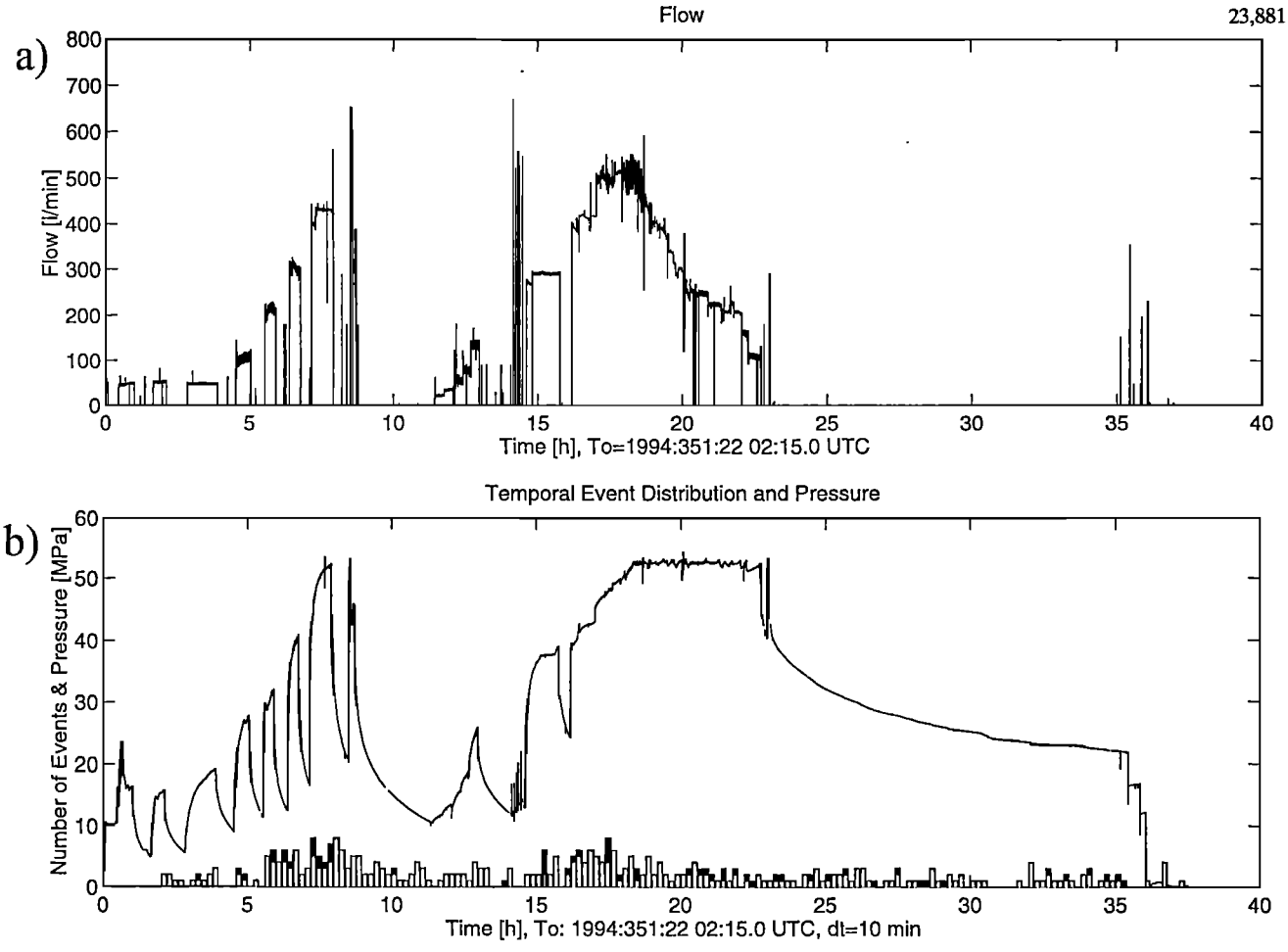

Figure 2. (a) Fluid flow and (b) pressure and induced seismicity (histogram, light shading) during the KTB Frac Experiment. Events with magnitude -1.0 or larger are shown in the solid histogram.

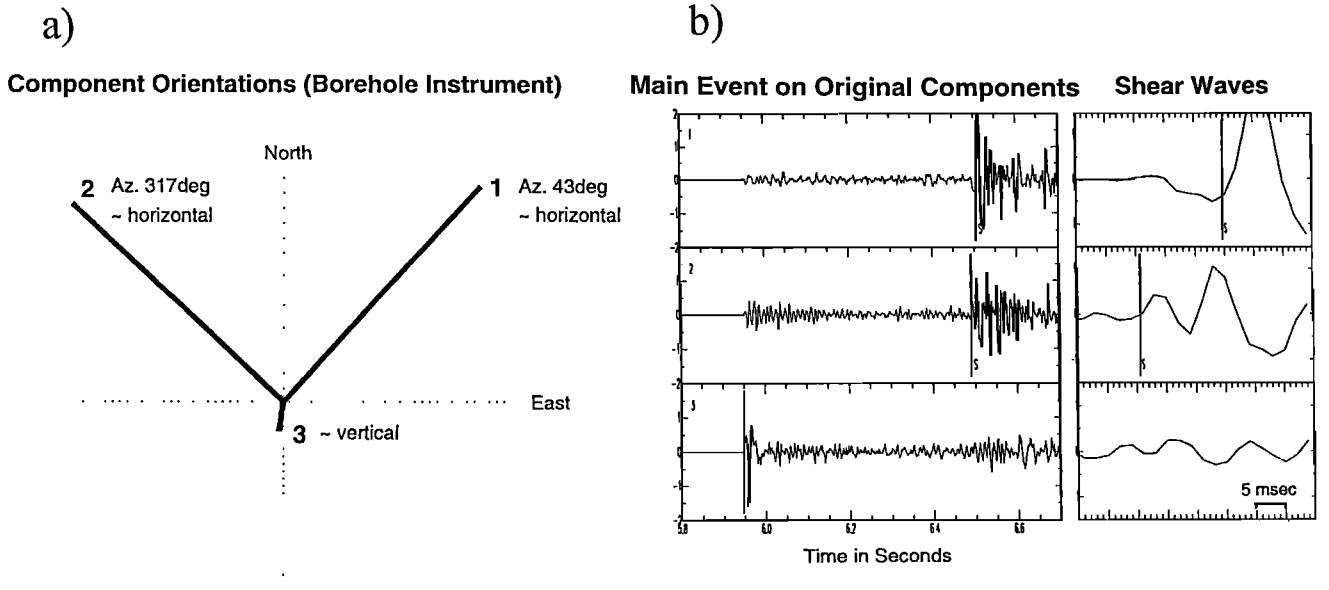

Figure 3. Borehole instrument orientation and waveforms of P and S waves for the main event: (a) the instrument orientation as seen from above (the third component is essentially vertical with positive upward). (b) The "Main Event" (origin time , day 352 at 1526:30.225 UTC) showing excellent P and S waveforms, recordable at such borehole sites. The S wave window is enlarged to show the typical S wave delay between the first (horizontal) component relative to the second. That delay was consistently observed for all events in the borehole data analyzed in this study. By chance, orientations of components 1 and 2 correspond more or less to the slow and fast directions (Az.=azimuth).

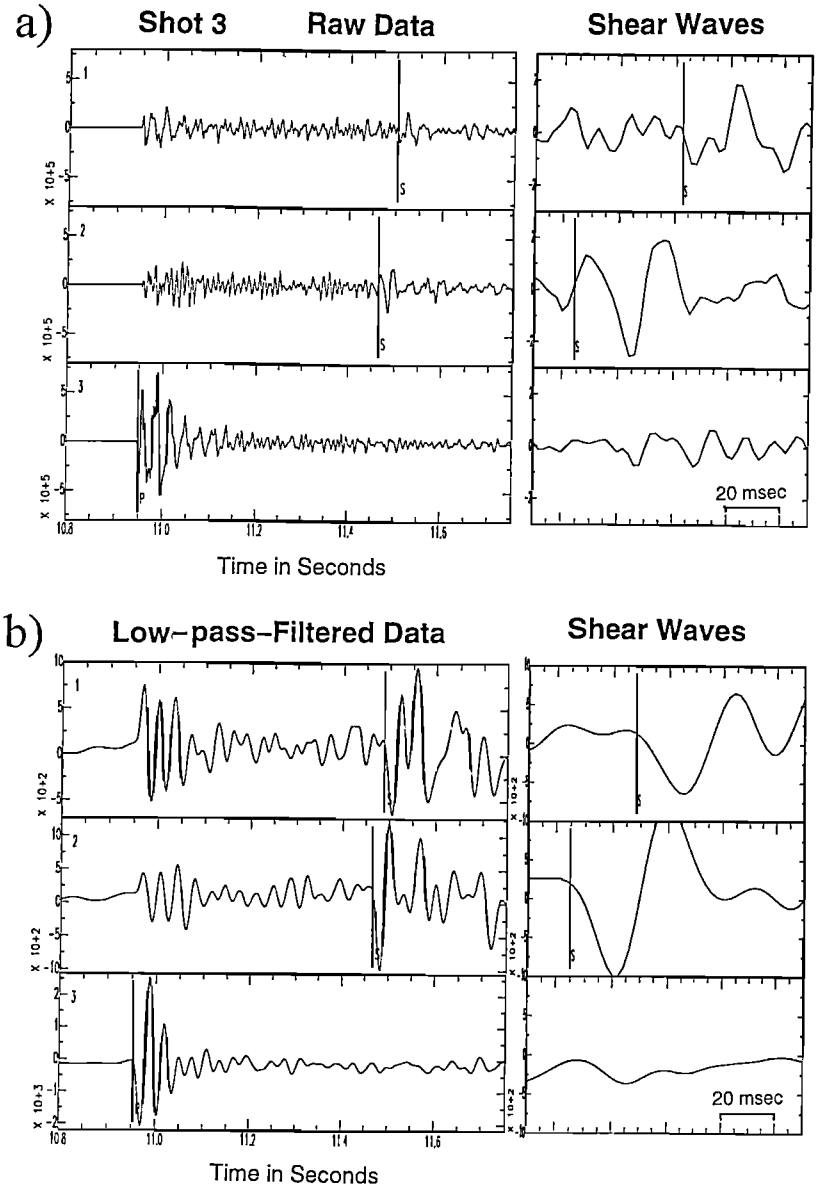

Figure 4. P and S waveforms for a surface shot (shot 3 on day 350 at 14:34:50.000 UTC) on the original components. Both raw data in Figure 4a and low-pass-filtered data (8Hz, causal) in Figure 4b show S phases arriving on the second component earlier than on the first. The fast polarization agrees quite well with the orientation of the second component. Manual determination of splitting delay is difficult though, as documented by the differing estimates of 39 ms and 23 ms for the splitting delay $t_{S2} - t_{S1}$, depending on whether the band-pass is used or not. If good accuracy is required, more sophisticated techniques must be used.

Seismic Network (GRSN) in southern Germany and the German Experimental Seismic System (GERESS) array, which is located $\sim$ 160 km to the southeast. Figure 3 shows a recording of that event on the three channels of the borehole instrument in the "Vorbohrung" (VB). The instrument orientation was determined by using P wave polarization data recorded from four surface shots. The instrument is tilted to the south in accordance with the local deviation of the borehole out of the vertical to the north. The early second component is seen for all events in this study, which is illustrated in Figure 4 using a calibration shot arriving from an almost perpendicular direction (Figure 1). Still, the S arrival is faster on the second component from the surface. This feature, an indication of anisotropy, is in general agreement with previous studies in the area [*Lüschen et al.*, 1991], and it also agrees with values for the crust in Central Europe [*Babuška and Cara*, 1991]. From Figure 3 we estimate the time separation between the shear waves on the two horizontal components as $\sim$ 14 ms for the main event. We obtain the relative difference $\delta\hat{\beta}$ between the two shear wave velocities β_1 and β_2, averaged over the path length (from HB to VB, Figure 1), if we can estimate the source-receiver distance D:

$$\delta\hat{\beta} \approx \frac{\beta_1(t_{S2}-t_{S1})}{D} \approx \frac{(t_{S2}-t_{S1})}{(t_{S1}-t_P)} \times \frac{\eta-1}{\eta} \approx 1.1\% \quad (1)$$

with the velocity ratio $\eta = \alpha/\beta_1 \approx \sqrt{3}$. This shows that we may obtain $\delta\hat{\beta}$ from measurement of three arrival times only with knowledge of η. We do not need to know the source-receiver distance D. The calibration shot (Figure 4) gives rise to much larger values of $\delta\hat{\beta}$ (1.9% or 3.2%) than the main event, no matter which estimate of $t_{S2}-t_{S1}$ we use. The most likely explanation is that effective anisotropy generally increases toward the surface, for example, due to increasing crack-induced anisotropy. This increase in anisotropy near the surface is consistent with several vertical profiling studies [e.g., *Aster and Shearer*, 1991]. There are indications that seismic anisotropy near the KTB borehole may also be affected by foliation directions [*Rabbel*, 1994], as was found to be the dominant effect under the GERESS array 160 km to the southeast [*Bokelmann*, 1995b]. However, even at 9 km depth, there may still be a component of crack-induced anisotropy if high fluid pressures are present. Figures 3 and 4 together give clear evidence that the time separation $t_{S2} - t_{S1}$ is caused by anisotropy and not by S-to-P conversion from a horizontal interface. The latter would predict a radially approximately north-south polarized fast arrival. Similarly, the effect of conversion off a dipping interface can be ruled out, since the structure dips to the northeast.

2.2. Spatial Distribution of Sources

All of the events occur in a spatially confined region: Figure 5 shows directions from the VB borehole instrument to the locations of the 35 strongest events (lower hemisphere plot). Incidence is always rather steep and all azimuths are in the third quadrant near 120°. Time separations $t_{S1} - t_P$ (approximately distance) are also given. The scatter indicates that distances of the events from the VB instrument vary by less than ±8%, which includes the statistical scatter of observations. In fact, we will see in section 2.3 that most of these events can be associated with several clusters of very tight spatial confinement.

An ideal experiment for testing the time-dependent anisotropy (TDA) hypothesis would consist of repeated identical sources (same focal mechanism and same source time function) at the same location. High-quality three-component receivers would be distributed such that identical ray paths through a crustal region are ob-

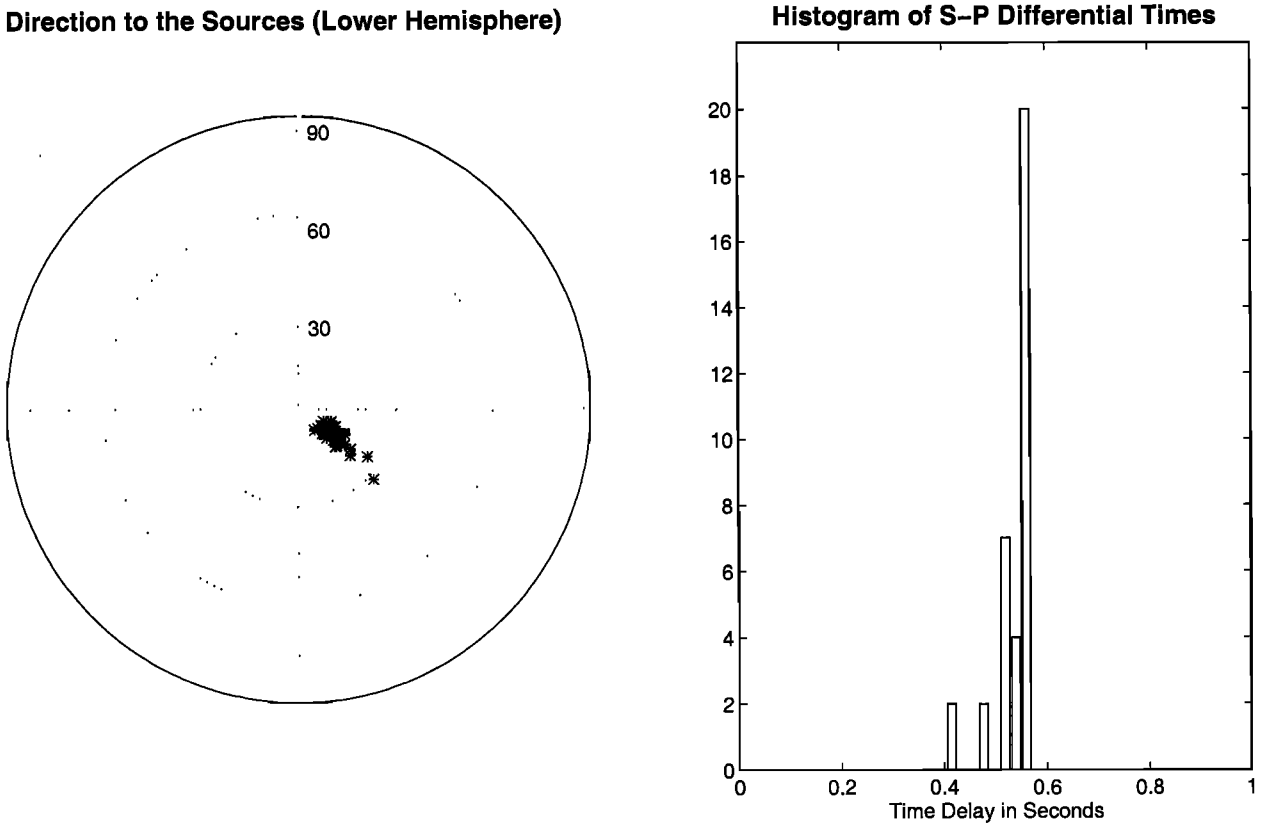

Figure 5. Receiver (borehole instrument) to source directions (lower hemisphere) and $t_{S1} - t_P$ differential time delays for the strongest 35 events. The events are within a spatially confined region as demonstrated by the small scatter in distance ($\approx t_{S1} - t_P$) and angles from the borehole instrument. Closer study shows that many of them form groups (clusters) of events having remarkable waveform similarity. This suggests special techniques of waveform matching to find subtle temporal changes of material parameters along the shared path.

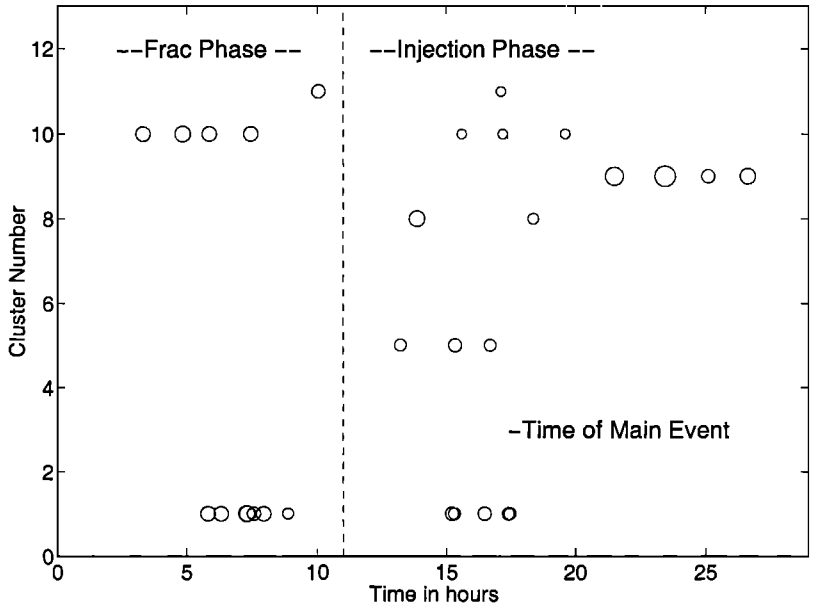

Figure 6. Temporal distribution (in hours) of five clusters of similar earthquakes at a required similarity level of at least 0.8 . The diameter of the symbols shows the magnitude of the events (maximum of -0.3, minimum of -1.2). A few other clusters (2,3,4,6,7) are too confined in time to be of interest in this study.

served, which may be described by a simple model. The receivers would preferably be located in deep boreholes to circumvent complex interferences from near-surface structure and to produce a high signal-to-noise ratio. Essentially, all of these criteria are met by the KTB Frac Experiment: Figure 3 shows that the three-component instruments record remarkable P and S waveforms, even at frequencies of 150 Hz. As sources we use data from well-defined clusters of events. We also have some prior knowledge of effective anisotropy in the region [*Lüschen et al.*, 1991; *Rabbel*, 1994]. The cluster analysis is described in section 2.3.

2.3. Event Clusters

We obtain nearly colocated events with similar source radiation by cluster analysis [*Schulte-Theis*, 1995] of the 100 strongest events. In that procedure, waveform similarity is measured by the maximum value of the cross correlation (we require at least 0.8). Successively, event pairs are distributed into different clusters of events. Generally, we obtain more clusters for longer time windows, but with a reduced maximum cross correlation value. For our purpose, we use time windows of 1.5 s, containing both P and S wave energy.

Could this procedure bias the time dependence analysis? Such a cluster analysis procedure would bias a possible time dependence to smaller values rather than to larger ones because event pairs displaying temporal variations are then less similar and might therefore be rejected from the cluster. On the other hand, the existence of highly similar doublets over some time interval shows that temporal variations can not be very large; instead, subtle variations are likely to be second-order effects that must be sought by highly accurate waveform comparison of the events within a cluster.

As will be seen in section 2.4, the degree of similarity between events of the same cluster is in fact remarkable. The existence of such "doublets" is well-known for seismic energy release across many different length scales, ranging from earthquake seismology [*Geller and Mueller*, 1980; *Poupinet et al.*, 1984; *Nadeau et al.*, 1995] to induced microseismicity [*Moriya et al.*, 1994].

The long time window in this study contains both the P and S phases and the coda and secondary phases. Highly similar events (and only these) must share the same path, since it is extremely unlikely that any other path can cause the same (kinematic and dynamic) pattern of reverberations at the receiver. Clearly, locations of such events are displaced from each other by at most a small fraction of the wavelength. *Geller and Mueller* [1980] estimated the maximum distance between two events in a doublet, which are similar up to a wavelength λ, as $\lambda/4$. This was confirmed by numerous authors thereafter, with some studies suggesting that $\lambda/4$ may be overly restrictive, perhaps due to the strong effect of some station site responses. By the same reasoning, these events must also have nearly identical focal mechanisms. Thus such events are ideal sources for testing the TDA hypothesis, since they give nearly identical signals propagating along nearly the same paths with appreciable time separations.

Out of the 100 strongest events, 57 can be associated with 11 clusters at the similarity level of at least 0.80 (cross correlation maximum). Seven of these clusters are quite confined in time, each lasting not longer than 5 hours. On the other hand, four clusters are more

spread out in time with durations of up to 12 hours. We may conceptually separate the time span of the experiment into three intervals, the frac phase and the early and late injection phases, which refer to the injection periods before and after the main event. Two of the clusters cover almost all three time intervals (see Figure 6). These are the most valuable clusters for our study, but we also use three other clusters with useful temporal coverage as they give us the opportunity to study the variation of shear wave splitting over time and also between these intervals.

2.4. Similarity of Waveforms

Figure 7 shows P and S waveforms for the four events in cluster 9. It is evident that both P and S waveforms are indeed very similar, at least where signal amplitudes

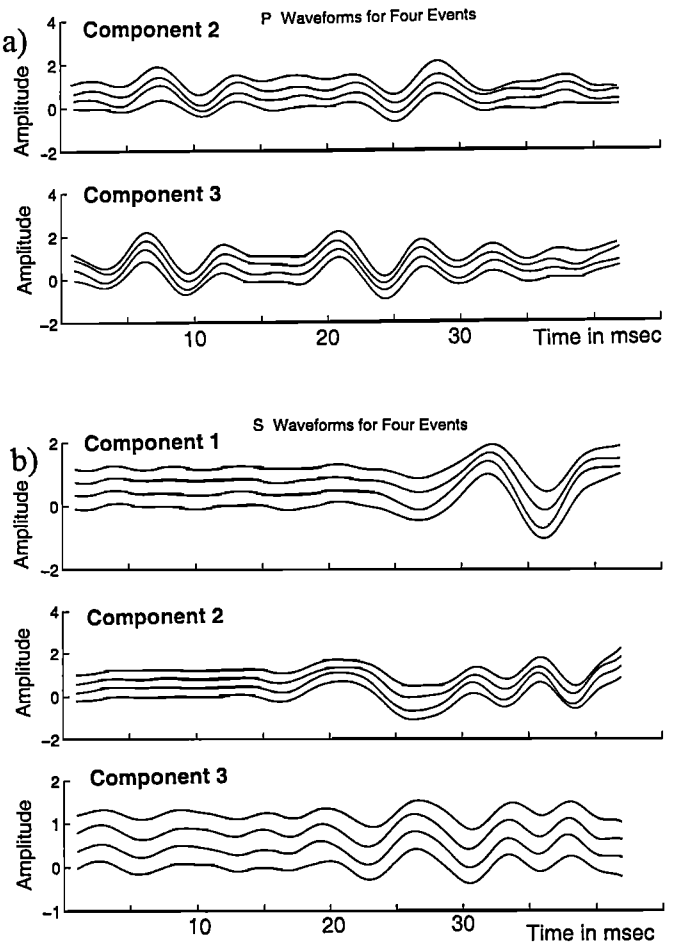

Figure 7. *P* and *S* waveforms for events in cluster 9, (a) P on the radial (2) and vertical (3) components, and (b) shows *S* on all components. Note the high degree of similarity of events within clusters. This is remarkable, considering that dominant frequencies are ~ 150 Hz. As a consequence, we may use detailed comparisons of such events to study time-dependent variations of medium properties. For this figure, raw waveform data have been interpolated, time-shifted, and amplitude-scaled only.

are sufficiently large. Shear waves agree very well on all components: To see subtle changes in the waveforms, closer inspection is required.

For the five clusters studied in this paper, Table 1 gives information for the associated events. The relative time delays $\Delta(t_{S2} - t_{S1})$ and $\Delta(t_{S1} - t_P)$ with respect to a reference event can be determined with high accuracy. Given estimates for the reference event, the time separations $t_{S2} - t_{S1}$ and $t_{S1} - t_P$ are determined to estimate the difference of shear wave velocities $\delta\hat{\beta}(t)$.

2.5. Waveform Matching Technique

In Figure 7 we have seen how remarkably similar waveforms are within the same cluster. Now we turn to the determination of relative delays between the phases for two events, particularly the relative splitting delay, the observable of prime interest in this paper. Are the small variations between the waveforms visible in Figure 7 systematic or not? To determine these variations, we display pairs of seismograms $\mathbf{u}_1(t)$ and $\mathbf{u}_2(t)$ (each component) using an initial alignment by waveform correlation on a large time window for each component, to roughly align the waveforms. For each component we compare the two seismograms in detail (see Figure 8). Figure 8 shows that waveforms are virtually identical aside from the small time shifts. Thus the waveform comparison is done most conveniently by a sliding cross correlation window, interpolating and monitoring the delay of the maximum [see also *Bokelmann*, 1992], depending on time. We obtain measurements of Δt_1 and Δt_2 with very high accuracy, far below the sampling interval of 1 ms. The capability of measuring such subsampling time delays is in agreement with other studies [see e.g., *Poupinet et al.*, 1984]: The limiting accuracy is controlled by waveform similarity, not by the sampling interval. We especially want to determine variations $\Delta(t_{S2} - t_{S1})$ of the delay $t_{S2} - t_{S1}$ between the two shear wave phases, which we obtain simply from the two quantities Δt_{S2} and Δt_{S1}, which we can determine very well

$$\Delta(t_{S2} - t_{S1}) = (t_{S2} - t_{S1}) - (t_{S2} - t_{S1})^{\text{ref}} =$$

$$(t_{S2} - t_{S2}^{\text{ref}}) - (t_{S1} - t_{S1}^{\text{ref}}) = \Delta t_{S2} - \Delta t_{S1}. \quad (2)$$

We use the delay estimates of the fast (S1) wave on the second component and the slow (S2) wave on the first component, since their amplitudes are largest on these components. Our delay estimates are composed of the cross correlation maximum lags averaged within the chosen time windows for the fast and slow shear wave phases.

The standard error of the delay between the two shear waves is $\delta = \sqrt{(\delta t_{S1})^2 + (\delta t_{S2})^2}$, with the scatter δt_{S1} and δt_{S2} of the delay relative to the reference event. This is a very simple but effective method for determining the relative splitting delay (or more generally between any two phases). The approach does not require

Table 1: Clusters of Similar Events Used in This Study[a]

Event[b]	Origin Time, Day:-UTC	Mag, ml	$\Delta^c t_{S1-P}$, ms	t^d_{S1-P}, ms	$\Delta^c t_{S2-S1}$, ms	t^d_{S2-S1}, ms	$\delta\hat{\beta}^e$, %
				Cluster 1			
(24)	352-0351·30.880	-0.8	0.00	579.00	0.00±0 05	14.50	1.058
25	352-0421:19.808	-0.8	-0 86	578.14	-0.18±0.07	14.32	1.047
16	352-0519:32.028	-0.7	-0.06	578.94	-0.10±0.03	14.40	1.051
19	352-0521.59 744	-0.7	-0.44	578.56	-0 10±0.06	14 40	1.052
76	352-0533.54 897	-1.2	-0.36	578.64	-0 15±0.05	14.35	1.048
34	352-0538·03.481	-0 9	-0.08	578.92	-0.15±0 05	14.35	1.048
29	352-0559 09.019	-0 8	-0.38	578.62	-0.10±0 06	14.40	1 052
67	352-0654:51.035	-1 1	-0.56	578.44	-0 13±0.05	14.37	1.050
43	352-1317:15.312	-0.9	-0.02	578.98	-0 26±0.06	14 24	1.040
49	352-1321:39.923	-1.0	-0.30	578.70	-0.23±0.08	14.27	1.042
39	352-1432:19.950	-0.9	0.16	579.16	-0 23±0.08	14.27	1.044
48	352-1527:21.615	-1 0	0.16	579.16	-0.34±0.07	14.15	1.036
47	352-1531·22.067	-1 0	-0.36	578.64	-0 37±0.12	14 13	1.032
				Cluster 10			
26	352-0121:10.691	-0 8	-0 10	554.40	-0.06±0.21	13.94	1.063
(17)	352-0252·37.508	-0 7	0.00	554.50	0.00±0.05	14.00	1 067
32	352-0353·53.902	-0 8	0.18	554 68	-0.08±0.07	13.92	1 060
27	352-0530:39.227	-0.8	-0.34	554.16	-0 09±0.18	13 91	1.061
86	352-1338:34.507	-1 2	-0.08	554.42	-0 14±0.25	13.86	1.057
75	352-1514 51 335	-1.2	-0 02	554 48	-0 13±0.20	13 87	1.057
97	352-1739:11.455	-1 2	-0.02	554 48	-0.39±0.13	13.61	1.037
				Cluster 9			
(8)	352-1931·49 888	-0 5	0.00	535.00	0.00±0 05	13.00	1 027
3	352-2129.03.308	-0 3	-0 02	534.98	-0 04±0.04	12 96	1 024
42	352-2308:11 075	-0.9	-0.04	534.96	0.06±0.08	13 06	1.032
18	353-0040 43.140	-0 7	0.06	535 06	0 02±0 04	13.02	1.029
				Cluster 11			
(35)	352-0805.07 707	-0 9	0 00	576.40	0 00±0.10	14.50	1.063
90	352-1510:50.274	-1 2	0 04	576.44	-0 19±0.22	14 31	1.049
				Cluster 5			
(61)	352-1115 20.956	-1 0	0 00	583.20	0 00±0.10	14.50	1.051
44	352-1323 04 487	-0 9	-0 32	582.88	-0 21±0.09	14.29	1.036
62	352-1445.21 357	-1 0	0 38	583 58	-0 01±0 14	14.49	1.049
				Cluster 8			
(20)	352-1153 46.358	-0 7	0 00	581.07	0 00±0 10	14 50	1.055
69	352-1625·46.000	-1.1	0 34	581 41	-0.05±0.22	14 45	1.050

[a] A few events are left out due to low signal/noise. These are events 77, 89, and 95 for cluster 1 and event 94 for cluster 9. Event 7 was discarded from cluster 5, because the magnitude was very different from the others (-0 4)

[b] Event numbers were given based on decreasing magnitude. Reference events (24, 17, 8, etc) are indicated by parentheses These events are used to compute $\Delta\hat{\beta}$ For these events, uncertainties for $\Delta(t_{S2}-t_{S1})$ are specified subjectively.

[c] Δ refers to the difference of a quantity with respect to the value for the reference event In both cases, (1) for determining the relative shear wave splitting delay and (2) the relative delay between faster S wave and P wave, the high-resolution method is used; accuracies for $\Delta^c t_{S2-S1}$ are typical for both.

[d] Here $t_{S2-S1} = t_{S2} - t_{S1}$ and $t_{S1-P} = t_{S1} - t_P$

[e] Here $\delta\beta$ is the difference in shear wave velocity between fast and slow velocity averaged over the ray path $\delta\hat{\beta} = \beta_2 - \beta_1/\beta_1$ with $\beta_1 = 6.2/\sqrt{3}$ km/s.

strong assumptions on the type of anisotropy causing the effects. Basically, the weak assumption it does make is that as elastic properties vary with time by a small amount, each observed wave phase changes primarily in travel time and amplitude but not in waveform shape. This assumption can be justified from Fermat's principle [see for example *Bokelmann*, 1992]. In particular, the approach makes no assumption about the relation between the waveforms of S1 and S2.

The only interactive part in the approach is in choosing time windows for the procedure to operate on. At that time the user is shown only the waveforms, and no indication of the time of the event, which prohibits subjective biases.

3. Results

Another waveform example from cluster 1 is displayed in Figure 9, which shows a much smaller delay $t_{S2} - t_{S1}$ compared with Figure 8. Figure 10 shows shows the results of this analysis for all events in cluster 1. Figure 10a compares different sets of time delay $t_{S1} - t_P$. Two sets of estimates obtained from manual picking scatter much more than the data set obtained from our procedure. Obviously, the uncertainty of estimates from the waveform matching is at least an order of magnitude smaller. The standard deviation is 0.3 ms. This confirms that (1) all event locations in the cluster are very near each other and (2) relative arrival times can be determined with accuracies of at least a third of the sampling interval which is 1 ms. The limits of uncertainty which can be reached is primarily determined by waveform similarity, not by the sampling rate [*Bokelmann*, 1995b]. The quantity $t_{S1} - t_P = Df(\beta_1, \alpha)$, with $f(\beta_1, \alpha) = [1/\beta_1 - 1/\alpha]$, which is computed for each event, depends on the source-receiver distance D and on medium velocities β_1 and α. Since D and the latter are unrelated quantities, we infer from the constancy of $t_{S1} - t_P$ for all events in cluster 1 that both $D \approx$ const and $f(\beta_1, \alpha) \approx$ const$= c$. The former means that distances vary by < 2 meters. The latter imposes a condition relating the variations of $\alpha(t)$ and $\beta_1(t)$. If we write $\alpha(t) = \alpha(0) + \Delta\alpha(t)$ and $\beta_1(t) = \beta_1(0) + \Delta\beta_1(t)$, we obtain

$$\Delta\alpha(t) \approx \frac{1 + c\beta_1(0)}{1 - c\beta_1(0)} \Delta\beta_1(t), \qquad (3)$$

which suggests $\Delta\alpha(t) \approx 2.4\Delta\beta_1(t)$. However, this can be explained more naturally, if both $\alpha(t)$ and $\beta_1(t)$ are constant. After all, the constancy of $f(\beta_1, \alpha)$ for varying α and β_1 may not be coincidental. Therefore it appears more likely that the temporal change occurs in the slower shear velocity β_2.

Observed shear wave splitting delays show a remarkable decrease, which is statistically significant. With estimates of $t_{S1} - t_P$ and $t_{S2} - t_{S1}$ we obtain estimates of $\delta\hat{\beta}$ from equation (1) using $\eta = \sqrt{3}$. The time de-

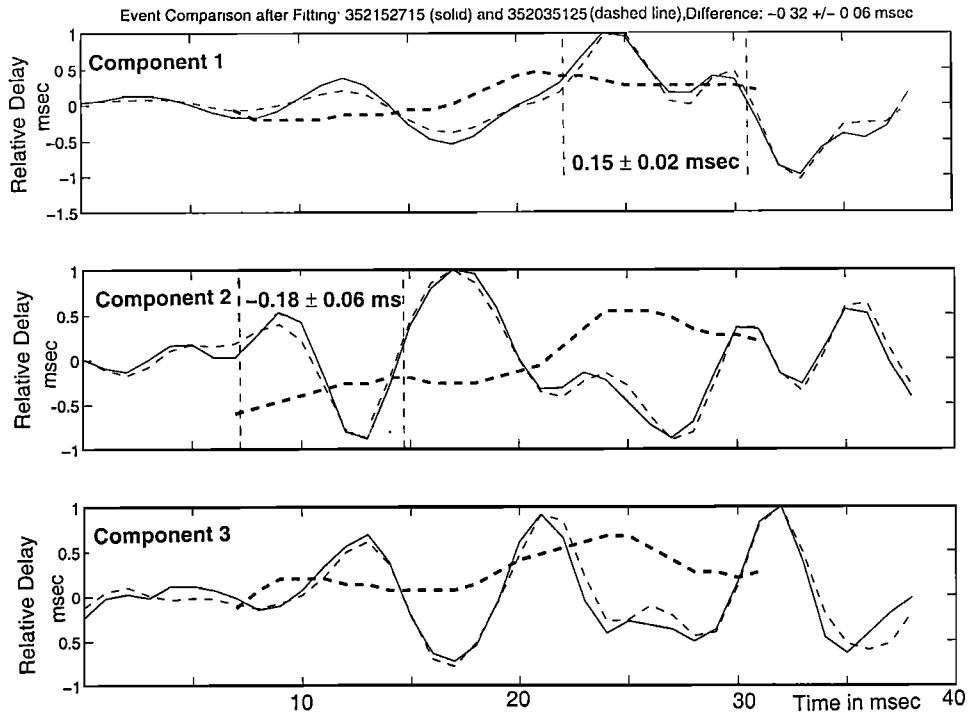

Figure 8. Illustration of the waveform matching technique for determining relative delays between two seismograms. Overlaying two three-component seismograms allows determination of the relative splitting delay $\Delta(t_{S2}-t_{S1}) = (t_{S2}-t_{S2}^{\mathrm{ref}})-(t_{S1}-t_{S1}^{\mathrm{ref}})$ (thick dashed line, in ms), The cross correlation operates on a sliding 15-ms window with a Hanning-type taper. Averaging over the windows shows by the vertical dashed lines results in a relative splitting delay $\Delta(t_{S2}-t_{S1})=-0.32 \pm 0.06$ ms. Clearly, this procedure allows subsample accuracy.

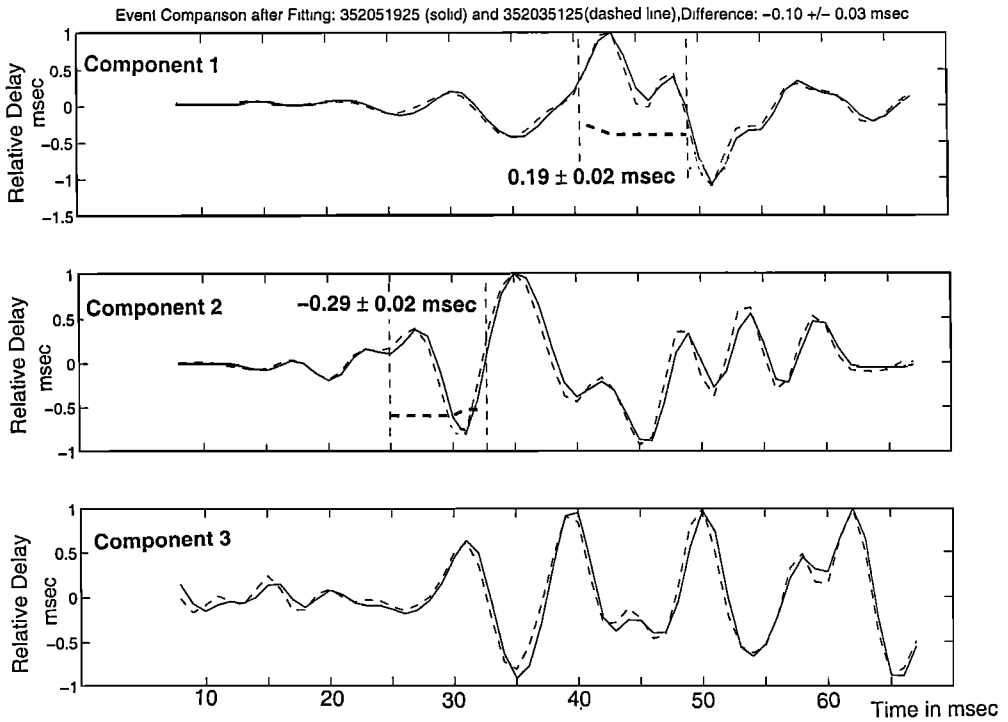

Figure 9. Waveforms and relative splitting delays for another event pair from cluster 1 (24-25). The time lag is shown only for the chosen time windows of S1 and S2 (display as in Figure 8). After approximate alignment the pair shows "earlier" time delays for both shear wave phases, while the example in Figure 8 showed a later S2. This documents an increasing time delay between the two shear waves from event to event.

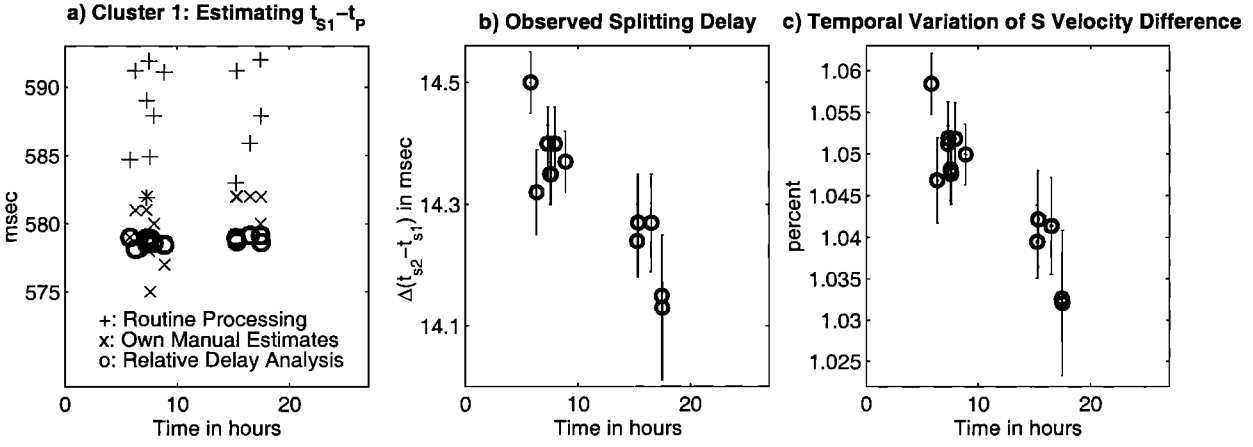

Figure 10. Results from cluster 1. (a) A comparison of different sets of $t_{S1} - t_P$ values for the events in cluster 1. Pluses indicate data from routine manual picking, crosses indicate data from an additional attempt using manual picking, and circles indicate values obtained from waveform matching. Clearly, the waveform matching produces standard errors, which are at least an order of magnitude smaller than those of manual picking, and distance variations of the events in cluster 1 are all within 10 meters (see text). (b) Observed values of relative splitting delay as a function of time during the experiment assuming $\eta = \sqrt{3}$ (time is given relative to 1994, day 351 at 2202:15.0 UTC), (c) The shear wave velocity difference in percent as a function of time. There is a clear decrease by $\sim$ 2% over just 12 hours.

pendence of that effect is clearly statistically significant with a variation of $\sim$ 2% within 12 hours. The effect of the time window choice has been extensively tested insuring that it has only minor influence on the result. Hence the method is objective in the sense that its results do not contain subjective biases.

3.1. Error Analysis

Which errors may affect estimates of $\delta\hat{\beta}$ and may perhaps cause artifacts? We note that results of $\delta\hat{\beta}$ are also affected by errors in reference event values [see also *Bokelmann*, 2000]. To understand its influence, consider that equation (1) is in our procedure used as

$$\delta\hat{\beta} = \frac{(t_{S2} - t_{S1})^{\text{ref}} + \Delta(t_{S2} - t_{S1})}{(t_{S1} - t_P)^{\text{ref}} + \Delta(t_{S1} - t_P)} \frac{\eta - 1}{\eta}, \qquad (4)$$

where the first terms in numerator and denominator (reference event values) are of size 10^2 and 10^3 ms. These values carry errors of the order of 1 ms. The other terms are of size 10^{-1} ms and carry errors of 10^{-2} ms. We are interested in the temporal variation of $\delta\hat{\beta}$ between two events, say $\delta\hat{\beta}_2 - \delta\hat{\beta}_1$. We choose the second event as the reference event and develop the denominator of $\delta\hat{\beta}_2$ keeping the first-order term (the next term is of order 10^{-6}). Then we see that the temporal variation is of size 10^{-2} (percent) with errors of order 10^{-3} arising primarily from the errors in $\Delta(t_{S1} - t_P)$. The reference events errors enter into the order 10^{-4}. Therefore, the temporal variation of $\delta\hat{\beta}$ is not affected by reference event errors. On the other hand, the reference event errors enter into the offset level of $\delta\hat{\beta}$ (absolute measurement), say $(\delta\hat{\beta}_1 + \delta\hat{\beta}_2)/2$, more strongly by an order of magnitude. The important feature is that the time dependence of $\delta\hat{\beta}$, say $\delta\hat{\beta}_2 - \delta\hat{\beta}_2$ is not affected.

In addition to the larger errors in the relative delays of the reference event differential arrival times, one must check effects of timing errors during the experiment. Generally, timing errors may be grouped into two types, both of which might affect the waveform data of our experiment: First, timing might suffer from a constant offset, and second, there might be a drift in the time signal, which would effectively spread or shrink the waveform data along the time axis. Since we exclusively use relative arrival times in this study, errors of the first type can not affect our analysis. On the other hand, a time drift with constant rate over the 0.6 s window containing both P and S phases, would spread or shrink waveforms and consequently affect estimates of $t_{S1} - t_P$ and $t_{S2} - t_{S1}$ similarly by a constant factor. That is the case if we use either equation (1) or (4). Equation (1) shows that through the quotient, this factor would cancel out and the estimates of $\delta\hat{\beta}$ are unaffected. For the data set in this paper, in fact, we are fortunate to have good knowledge of the true timing signal during the experiment. Variation in this timing signal is only of the order of microseconds. However, also in the case of a less-known timing signal, the suggested type of analysis is robust in the sense that it offers at the same time very high accuracies and is also insensitive to timing errors, which may easily bias other types of studies of time-dependent effects, at least if the size of the temporal variations are of the order of only a few percent.

3.2. Other Clusters

The same waveform analysis was applied to data from the other clusters. For cluster 10, waveform similarity is generally somewhat smaller than for cluster 1 (Table 1). Nevertheless, we obtain a similar result: small shear wave splitting variations for event pairs with time separations of just a few hours. For larger separation, splitting delays vary more. Differential times $t_{S1} - t_P$ again show a near constancy with time, while splitting delays decrease significantly. The $\delta\hat{\beta}$ clearly varies with time consistent with the results of cluster 1, although uncertainties are larger for cluster 10. Clusters 1 and 10 essentially have similar temporal coverage and are hence easily comparable: Both consistently show that the difference between the two shear wave velocities decreases with time.

How does $\delta\hat{\beta}$ behave after the main event? The largest remaining cluster, cluster 9, covers a time interval of 11 hours after the main event. Figure 11 shows waveforms and relative splitting delays for an example event pair from cluster 9. Waveform similarity for events in cluster 9 is remarkable. Visually comparing the event pairs, we notice that time variation of shear wave splitting is clearly small. This is also apparent in the results (Table 1), where uncertainties are very small, reflecting the excellent similarity. Variations of differential times $t_{S1} - t_P$ are never larger than 0.6 ms. Also the shear wave delays hardly vary: Temporal variation of shear wave splitting in the latter part of the experiment is negligible for cluster 9.

3.3. Total Temporal Variation

In order to study temporal variations along the total duration of the experiment we need to take into account the perhaps different absolute level of $\delta\hat{\beta}$ for different clusters. A conservative approach of doing this is to fit a straight line to the values of $\delta\hat{\beta}$ for each event and to constrain these extrapolations to coincide in the center of overlapping time intervals or the center of the gap for nonoverlapping time intervals. This procedure gives the temporal variation shown in Figure 12, where the adjustment is in agreement with the data for the three small clusters covering the transition (Table 1), which shows a mild decrease in $\delta\hat{\beta}$. The total variation is of the order of 2%. Interestingly, the difference of shear wave velocities decreases till the main event and stays constant after that. Polarization directions do not show such systematic changes within clusters, neither for P waves nor for the faster S waves.

4. Discussion

The main results from this study are (1) that the medium properties do in fact vary with time and (2) that we may indeed observe such effects. However, it is also of great interest to understand the nature of this time dependence. We will in the following section discuss possible causes for the temporal variation which are (1) the injected fluid, and (2) changes in mechanical stress due to (a) the induced seismicity or (b) solid

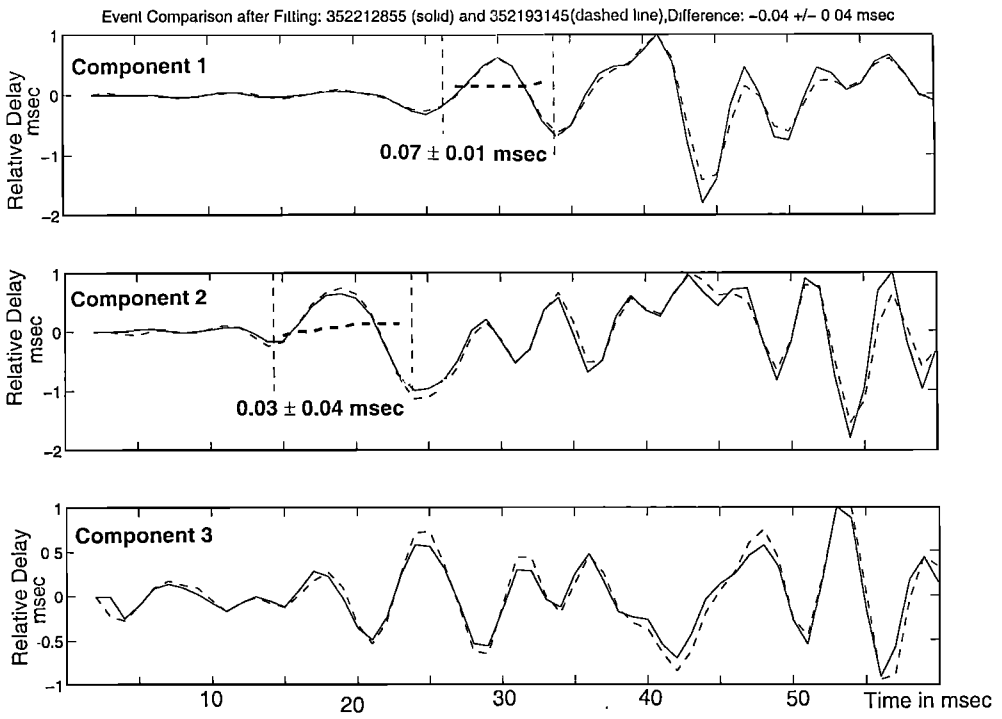

Figure 11. Waveforms and relative splitting delays for an example event pair from cluster 9 (events 8 and 3). The display is similar to Figure 8.

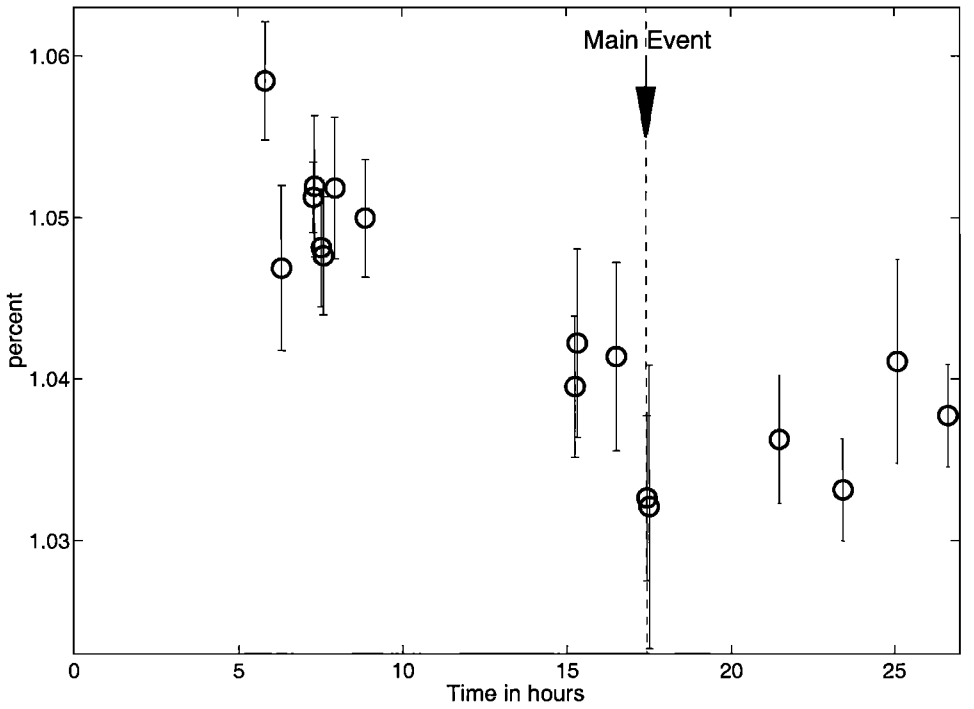

Figure 12. Temporal variation of shear wave splitting over the length of the experiment (clusters 1 and 9). See the text for discussion.

Earth tides. Can any of these factors explain a variation of $\sim 2\%$ in $\delta\hat{\beta}$ (or alternatively in η)?

Figure 13 shows the volume of the first Fresnel zone for the dominant frequency of 150 Hz, which consists of all points giving rise to time delays $\Delta T \leq T/4$ relative to the first arrival time. A good approximation to the wave field can be made by assuming that only this volume contributes to the data [*Snieder and Lomax*, 1996]. The volume of that body is approximately 10^8 m^3. Prior to the main event, about 126 m^3 of fluid was injected at 9 km depth. We take the most favorable view and assume that all fluid propagates into the Fresnel volume where it can affect the observations. Although unlikely, it gives a viable argument about whether the injected fluid can explain the observations at all. The 126 m^3 of fluid may change the mean fluid content in the volume (mean excess porosity) by 10^{-6}. Can such a small change in fluid content cause sufficiently large variations in η? Randomly oriented circular cracks as computed from a self-consistent approach following *O'Connell and Budiansky* [1974] would require a mean excess porosity of the order of a few percent to explain the temporal variation of 2%. This is 4 orders of magnitude larger than can be explained by the injected fluid (10^{-6}). Thus the injected fluid cannot explain the observed effects, at least if the pore spaces are isotropic. In the following section we will be dealing with anisotropic pore spaces.

4.1. Tectonic Release

The hydraulic fracturing set of a large number of seismic events with strike-slip mechanism [*Zoback and Harjes*, 1997]. These are consistent with the regional stress field (NW-SE compression), suggesting that a substantial fraction of the released seismic energy is due to a relaxation of tectonic stress. Changes of stress differences may have a considerable effect on effective anisotropy [e.g., *Zatsepin and Crampin*, 1997], especially when fluid-filled cracks are present throughout the medium. Events in this study produced stress drops on the order of 10^5 Pa (bars) and fracture sizes of few tens of meters. On the other hand, the sensitivity of relative velocity changes with respect to stress changes has been suggested to be of order 10^{-8} or even 10^{-7} Pa^{-1} near the surface [*De Fazio et al.*, 1973]. A study in southern Germany using continuous man-made signals [*Baisch and Bokelmann*, 1999] produced an upper bound of 10^{-8} Pa^{-1}. With an average stress drop of several 10^4 Pa (assuming that stress release occurs on a "fault plane" throughout the Fresnel volume) we may, in principle, explain the magnitude of the observed effects by tectonic stress change in an anisotropic medium containing fluid-filled cracks. This mechanism should also explain further characteristics of the observations, namely that (1) $\delta\hat{\beta}$ decreases with increasing stress drop and (2) the variation occurs (most likely) in the slower S velocity β_2, which is polarized in NW-SE direction.

Figure 14 illustrates our interpretation. The cracks are oriented in σ_1 direction, perpendicular to σ_3. Figure 14b shows that tectonic stress drop causes the normal stress on the cracks $\sigma_n = \sigma_3$ to increase. This leads to a flattening of the cracks (decrease of aspect ratio α). Figure 14c presents the results from a model of random aligned cracks [*Hudson*, 1981]. Specifically, the two S velocities are shown for a number of aspect ratios. We

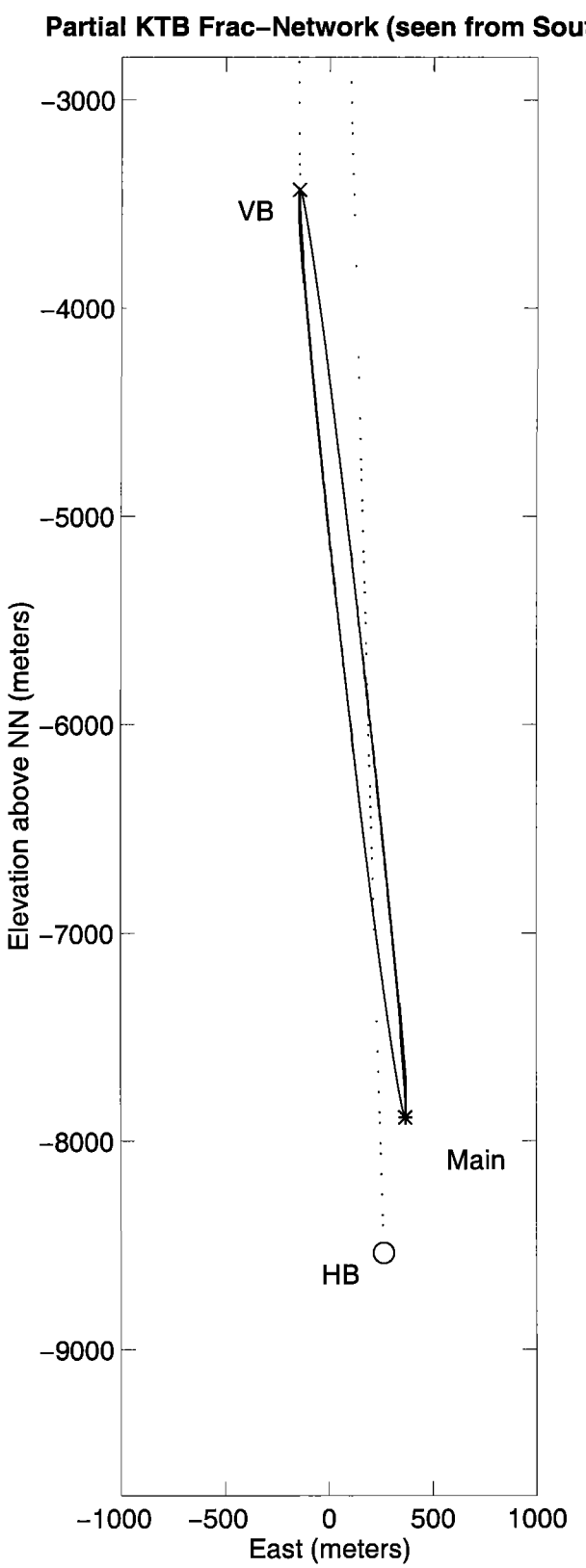

Figure 13. Closer view of the geometry of the experiment: A circle of 50 m radius is drawn around the point of fluid injection (Hauptbohrung HB); The rays propagate from the source location, for example, "main" to the Vorbohrung VB. The first Fresnel volume (zone) is shown for 150 Hz (100 times exaggerated in width). The observed shear wave effect can be interpreted as being due to contributions from this Fresnel volume.

see that indeed $\delta\beta = \beta_1 - \beta_2$ decreases for decreasing aspect ratios for all angles which produce considerable S wave splitting. Furthermore, this model predicts that the slower S wave velocity β_2 varies, while β_1 is constant. We can match the size of the observations by a 1% change of the aspect ratio if the angle of propagation is 45° from the symmetry axis. This would be the case if the cracks were roughly aligned with the foliation, which dips with $\sim$ 50° to the northeast [*Harjes et al.*, 1997]. A more vertical orientation of the cracks would require larger changes in aspect ratio in this model.

We illustrated that the nature of the velocity change can be explained by a change in mean aspect ratio of the cracks. The crack density was chosen as $\epsilon = 0.05$. This model is certainly simplistic. A more realistic treatment would also allow a varying orientation distribution of open cracks [e.g., *Zatsepin and Crampin*, 1997]. However, this simple crack model does qualitatively reproduce the relevant features of the observed temporal variation.

4.2. Solid-Earth Tides

Another stress field which we need to address is that arising from solid Earth tides, which give rise to periodic changes of stress within the crust. These are of the order of 10^3 Pa, smaller than the coseismic stress changes. However, they act throughout the entire crust. Unfortunately, the time duration of our experiment was not long enough to rule out a periodic change of $\delta\hat{\beta}$ with period of about 1/day and 2/day directly. Therefore the possibility of tidal effects cannot be ruled out entirely given the uncertainties involved. A longer-time observation of shear wave splitting using doublet data would be an important test to better distinguish this effect from tectonic causes. In any case, such a test gives a measure for the extent of open compliant cracks in deeper levels of the crust. The possibility for such a long-time monitoring of seismic velocities has been addressed for continuously generated (machine) signals from the surface [*Bokelmann and Baisch*, 1999; *Baisch and Bokelmann*, 1999].

4.3. Comparison With Other Studies

Poupinet et al. [1984] found temporal variations of S velocities by $\sim$ 0.2% before and after a magnitude 5.9 event in California using a coherence-based method operating on full seismograms of events with similar waveform. In contrast to our paper, the split shear waves were not specifically addressed, but that method is also capable of resolving very small time shifts. In fact, the size of temporal variation that it suggests is similar to the effect in our paper. The ideal approach to studying time-dependent variations is certainly the approach using doublets to eliminate alternative apparent time dependences (distance variation of events; variation of focal mechanism), unless there are sources which are indeed fixed in space [*Bokelmann*, 1997]. A number of studies have claimed to observe temporal varia-

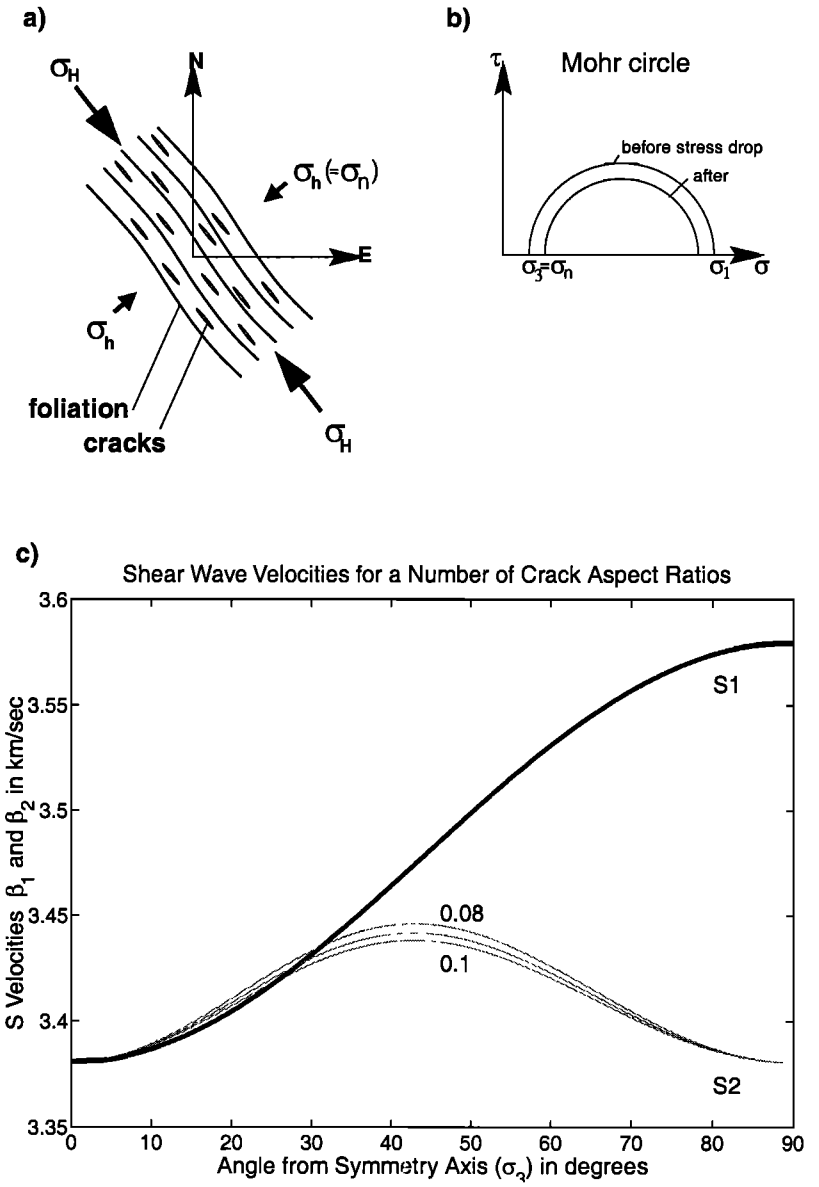

Figure 14. (a) Orientation of maximum and minimum horizontal compressive stress (σ_H, σ_h). Cracks opening normal to σ_3 (= σ_h if σ_2 vertical) have similar strike as the foliation direction. (b) Increase in crack normal stress $\sigma_n = \sigma_3$ during a quake, leading to a flattening of the cracks (decreasing aspect ratio α). (c) Dependence of S velocities on crack aspect ratio. Decreasing aspect ratio α produces a decrease in $\delta\beta$ for angles larger than 30°. Note that the slower S velocity β_2, which is polarized in NE-SW direction, is predicted to vary, while the faster β_1 is constant.

tions, mostly in the ratio α/β [*see Lukk and Nersesov*, 1978]. However, observation of small variations poses very strong requirements on eliminating errors from distance variation and timing, which are very difficult to satisfy with other methods than ones based on waveform correlation of doublets. Also for the Anza Gap data set, seismic doublets have been used to show that temporal variations are at most 5 to 10% [*Aster et al.*, 1990], which disagrees with large temporal variations which were claimed by other researchers [*Peacock et al.*, 1988; *Crampin et al.*, 1990]; on the other hand, that upper bound does not preclude temporal variation of the size observed in our study or in that of *Poupinet et al.* [1984]. In our experience, it is often difficult to unambiguously determine time delays between fast and slow shear wave phases by visual inspection of a single three-component seismogram. In fact, initial estimates of shear wave splitting from our data, which were based on visual analysis also showed large excursions. After allowing only clusters of doublets and performing the objective procedure, temporal variations almost vanished and the stable smaller-scale pattern emerged.

5. Conclusions

The main result of this study is that shear wave splitting has been observed to vary with time at a depth level of 4 to 9 km. The analysis procedure is objective in the sense that subjective influences are eliminated; importantly, the procedure is able to determine temporal variations of the relative shear wave velocity difference with very high accuracies ($\approx 10^{-4}$). The anisotropy itself, as documented by shear wave splitting, has a size of ~1% and is generally consistent with previous observations. Intriguingly, shear wave splitting decreases for $\sim$ 12 hours and is essentially constant afterward. No assumption is made that the events are colocated. Nevertheless, the analysis showed that the events actually do occur very close to each other, confirming the hypothesis of similar events. No progressive change of source location is apparent from either the time delays nor the P wave polarizations.

It is interesting that the change in medium configuration occurs apparently almost instantaneously, with a lag of at most a few hours. The injected fluid volume cannot explain the temporal change by itself. On the other hand, the effect of the stress drop due to induced seismicity may possibly explain the data if fluid-filled cracks are present at depth larger than 4 km. A longer-time experiment in a deep borehole as KTB would help to further understand the mechanisms of temporal variation in the Earth's crust.

Acknowledgments. We wish to thank the KTB team which assisted in performing the injection experiment. Markus Janik, Hartwig Schulte-Theis, Matthias Bahlo, and Thorsten Büsselberg provided valuable help in analyzing the waveform data. We profited from discussions with Fritz Rummel. Reviews by George Helffrich, Peter Shearer, and an anonymous reviewer greatly improved the manuscript.

References

Ando, M., Y. Ishikawa, and F. Yamazaki, Shear wave polarization anisotropy in the upper mantle beneath Honshu, Japan, *J. Geophys. Res., 88*, 5850-5864, 1983.

Aster, R.C., and P.M. Shearer, High-frequency borehhole seismograms recorded in the San Jacinto fault zone, *Bull. Seismol. Soc. Am., 81*, 1057-1080, 1991.

Aster, R.C., P.M. Shearer, and J. Berger, Quantitative measurements of shear wave polarizations at the Anza seismic network, Southern California: Implications for shear wave splitting and earthquake prediction, *J. Geophys. Res., 95*, 12,449-12,473, 1990.

Babuška, V., and M. Cara, *Seismic Anisotropy in the Earth*, Kluwer Acad., Norwell, Mass., 1991.

Baisch, S., and G.H.R. Bokelmann, Spectral analysis with incomplete time series: An example from seismology, *Comput. Geosci., 25*, 739-750, 1999.

Bokelmann, G.H.R., Upper and lower mantle small-scale heterogeneity studied by systematic analysis of portable broadband waveforms and travel times, Ph.D. thesis, Princeton Univ., Princeton, N.J., 1992.

Bokelmann, G.H.R., *P*-wave array polarization analysis and effective anisotropy of the brittle crust, *Geophys. J. Int., 120*, 145-163, 1995a.

Bokelmann, G.H.R., Azimuth and slowness deviations from the GERESS regional array, *Bull. Seismol. Soc. Am., 85*, 5, 1456-1463, 1995b.

Bokelmann, G.H.R., Messung zeitlicher Variationen von Wellengeschwindigkeiten in der Erdkruste, *Mitt. Dtsch. Geophys. Ges., 3*, 6-12, 1997.

Bokelmann, G.H.R., A method for resolving small temporal variations of effective elastic properties, *SEG Special Volume*, in press, 2000.

Bokelmann, G.H.R., and S. Baisch, Nature of narrow-band signals at 2.083 Hz, *Bull. Seismol. Soc. Am., 89*, 156-164, 1999.

Crampin, S., and S.V. Zatsepin, Changes of strain before earthquakes; The possibility of routine monitoring of both long-term and short-term precursors, *J. Phys. Earth, 45*, 1, 41-66, 1997.

Crampin, S., D.C. Booth, R. Evans, S. Peacock, and S.B. Fletcher, Changes in shear wave splitting at Anza near the time of the North Palm Springs earthquake, *J. Geophys. Res., 95*, 11,197-11,212, 1990.

De Fazio, T.L., K. Aki, and J. Alba, Solid Earth tide and observed change in the in situ seismic velocity, *J. Geophys. Res., 78*, 1319-1322, 1973.

Geller, R.J., and C.S. Mueller, Four similar earthquakes in central California, *Geophys. Res. Lett., 7*, 821-824, 1980.

Gupta, I.N., Premonitory variations in *S*-wave velocity anisotropy before earthquakes in Nevada, *Science, 182*, 1129-1132, 1973.

Harjes, H.P., et al., Origin and nature of crustal reflections: results from integrated seismic measurements at the KTB superdeep drilling site, *J. Geophys. Res., 102*, 18,267-18,288, 1997.

Hess, H. H., Seismic anisotropy of the uppermost mantle under oceans, *Nature, 203*, 629-631, 1964.

Hudson, J.A., Wave speeds and attenuation of elastic waves in material containing cracks, *Geophys. J. R. Astron. Soc., 64*, 133-150, 1981.

Lukk, A.A., and I.L. Nersesov, Character of temporal changes in the velocities of elastic waves in the Earth's crust of the Garm region, *Izv. Phys. Sol. Earth, 14*, 387-396, 1978.

Lüschen, E., W. Söllner, A. Hohrath, and W. Rabbel, Integrated *P*- and *S*-wave borehole experiments at the KTB deep drilling site in the Oberpfalz area, in *Continental Lithosphere: Deep Seismic Reflections, Geodyn. Ser.*, vol. 22., edited by R. Meissner et al., pp. 121-133, AGU, Washington, D.C., 1991.

Moriya, H., K. Nagano, and H. Niitsuma, Precise source location of AE doublets by spectral matrix analysis of triaxial hodogram, *Geophysics, 59*, 36-45, 1994.

Nadeau, R.M., W. Foxall, and T.V. McEvilly, Clustering and periodic recurrence of microearthquakes on the San Andreas Fault at Parkfield, California, *Science, 267*, 503-507, 1995.

O'Connell, R.J., and B. Budiansky, Seismic velocities in dry and saturated cracked solids, *J. Geophys. Res., 79*, 5412-5426, 1974.

Peacock, S., S. Crampin, D.C. Booth, and J.B. Fletcher, Shear-wave splitting in the Anza seismic gap, southern California: Temporal variations as possible precursors, *J. Geophys. Res., 93*, 3339-3356, 1988.

Poupinet, G., W.L. Ellsworth, and J. Frechet, Monitoring velocity variations in the crust using earthquake doublets: An application to the Calaveras fault, California, *J. Geophys. Res., 89*, 5719-5731, 1984.

Rabbel, W., Seismic anisotropy at the Continental Deep Drilling Site (Germany), *Tectonophysics, 232*, 329-341, 1994.

Ryall, A, and W. Savage, *S* wave splitting: Key to earthquake prediction?, *Bull. Seismol. Soc. Am.*, *64*, 1943-1951, 1974.

Schulte-Theis, H., Automatische Lokalisierung und Clusteranalyse regionaler Erdbeben, Ph.D. Thesis, Univ. Bochum, Bochum, Germany, 1995.

Snieder, R., and A. Lomax, Wavefield smoothing and the effect of rough velocity perturbations on arrival times and amplitudes, *Geophys. J. Int.*, *125*, 796-812, 1996.

Zatsepin, S.V., and S. Crampin, Modelling the compliance of crustal rock, I, Response of shear wave splitting to differential stress, *Geophys. J. Int.*, *129*, 477-494, 1997.

Zoback, M.D., and H.P. Harjes, Injection-induced earthquakes and crustal stress at 9 km depth at the KTB deep drilling site, Germany, *J. Geophys. Res.*, *102*, 18,477-18,491, 1997.

G.H.R. Bokelmann, Department of Geophysics, Stanford University, Stanford, CA 94305-2215. (goetz@pangea. stanford.edu)

H.-P. Harjes, Institut für Geophysik, Ruhr-Universität, Universitätsstr. 150, D-44780 Bochum, Germany. (harjes @geophysik .ruhr-uni-bochum.de)

(Received November 11, 1999; revised May 4, 2000; accepted June 9, 2000.)